Quantitative PET Imaging of Tissue Factor Expression Using ^{18}F-Labeled Active Site–Inhibited Factor VII

Carsten H. Nielsen[1,2], Maria Erlandsson[2], Troels E. Jeppesen[2], Mette M. Jensen[1,2], Lotte K. Kristensen[1,2], Jacob Madsen[2], Lars C. Petersen[3], and Andreas Kjaer[2]

[1]Minerva Imaging, Copenhagen, Denmark; [2]Department of Clinical Physiology, Nuclear Medicine & PET and Cluster for Molecular Imaging, Rigshospitalet and University of Copenhagen, Copenhagen, Denmark; and [3]Haemostasis Biology, Novo Nordisk A/S, Maaloev, Denmark

Tissue factor (TF) is upregulated in many solid tumors, and its expression is linked to tumor angiogenesis, invasion, metastasis, and prognosis. A noninvasive assessment of tumor TF expression status is therefore of obvious clinical relevance. Factor VII is the natural ligand to TF. Here we report the development of a new PET tracer for specific imaging of TF using an ^{18}F-labeled derivative of factor VII. **Methods:** Active site–inhibited factor VIIa (FVIIai) was obtained by inactivation with phenylalanine–phenylalanine–arginine–chloromethyl ketone. FVIIai was radiolabeled with *N*-succinimidyl 4-^{18}F-fluorobenzoate and purified. The corresponding product, ^{18}F-FVIIai, was injected into nude mice with subcutaneous human pancreatic xenograft tumors (BxPC-3) and investigated using small-animal PET/CT imaging 1, 2, and 4 h after injection. Ex vivo biodistribution was performed after the last imaging session, and tumor tissue was preserved for molecular analysis. A blocking experiment was performed in a second set of mice. The expression pattern of TF in the tumors was visualized by immunohistochemistry and the amount of TF in tumor homogenates was measured by enzyme-linked immunosorbent assay and correlated with the uptake of ^{18}F-FVIIai in the tumors measured in vivo by PET imaging. **Results:** The PET images showed high uptake of ^{18}F-FVIIai in the tumor regions, with a mean uptake of 2.5 ± 0.3 percentage injected dose per gram (%ID/g) (mean ± SEM) 4 h after injection of 7.3–9.3 MBq of ^{18}F-FVIIai and with an average maximum uptake in the tumors of 7.1 ± 0.7 %ID/g at 4 h. In comparison, the muscle uptake was 0.2 ± 0.01 %ID/g at 4 h. At 4 h, the tumors had the highest uptake of any organ. Blocking with FVIIai significantly reduced the uptake of ^{18}F-FVIIai from 2.9 ± 0.1 to 1.4 ± 0.1 %ID/g ($P < 0.001$). The uptake of ^{18}F-FVIIai measured in vivo by PET imaging correlated ($r = 0.72$, $P < 0.02$) with TF protein level measured ex vivo. **Conclusion:** ^{18}F-FVIIai is a promising PET tracer for specific and noninvasive imaging of tumor TF expression. The tracer merits further development and clinical translation, with potential to become a companion diagnostics for emerging TF-targeted therapies.

Key Words: positron emission tomography (PET); PET/CT; tissue factor (TF); pancreatic cancer; ^{18}F; active site inhibited factor VII (FVIIai); molecular imaging; cancer; oncology

J Nucl Med 2016; 57:89–95
DOI: 10.2967/jnumed.115.154849

Tissue factor (TF) is a 47-kDa transmembrane protein that binds factor VII (FVII) with high affinity. The resulting complex initiates the extrinsic coagulation cascade essential for normal hemostasis. On binding to TF, the zymogen FVII gets activated to the serine protease, FVIIa; and the TF:FVIIa complex further activates factor X, eventually leading to thrombin generation and hemostasis.

In addition to its role in coagulation, TF plays a central role in cancer progression, angiogenesis, invasion, and hematogenous metastatic dissemination. Many tumors express various levels of cell surface TF, and the TF:FVIIa complex has been shown to activate protease-activated receptor 2 and through intracellular signaling to induce an antiapoptotic effect as well as to enhance tumor growth, migration, and angiogenesis. In addition, TF:FVIIa more indirectly facilitates metastatic dissemination through thrombin generation and PAR1 signaling (*1–4*).

Clinically, TF is overexpressed in several cancers including glioma, breast, colorectal, prostate, and pancreatic cancer (*5–8*). Within ductal adenocarcinoma of the pancreas it has been shown that TF, measured by immunohistochemistry, correlates with histologic grade and is a prognostic marker of overall survival (*9,10*).

Targeting TF has proven effective as a cancer therapy in preclinical models. Yu et al. demonstrated that silencing of TF by small interfering RNA reduced tumor growth in a mouse model of colorectal cancer (*11*). Using an immunoconjugate with FVII as the binding domain, Hu et al. suppressed tumor growth in a human melanoma xenograft mouse model (*12*). Ngo et al. and Versteeg et al. demonstrated that anti-TF antibodies inhibited metastasis in an experimental metastasis model and suppressed tumor growth in a breast cancer model (*13,14*). Targeting of TF with an antibody-drug conjugate was recently shown to have a potent and encouraging therapeutic effect in murine cancer models, including patient-derived xenograft models (*15*). A noninvasive method for specific assessment of tumor TF expression status would be valuable. Such a tool would be clinically relevant for guidance of patient management and as companion diagnostics for emerging TF-targeting therapies.

Here we report the development and in vivo testing of a new PET tracer for specific imaging of TF using FVIIai labeled with ^{18}F. FVIIai (molecular weight, 50 kDa), which binds to TF with an affinity approximately 5-fold higher than FVIIa (*16*), was radiolabeled with ^{18}F by *N*-succinimidyl 4-^{18}F-fluorobenzoate (^{18}F-SFB; molecular weight, 237 Da). The in vivo properties of ^{18}F-FVIIai for PET imaging were evaluated in a mouse model of human pancreatic cancer using small-animal PET/CT. The uptake of

Received Mar. 24, 2015; revision accepted Aug. 19, 2015.
For correspondence or reprints contact: Andreas Kjaer, Department of Clinical Physiology, Nuclear Medicine & PET, Rigshospitalet, KF-4012, Blegdamsvej 9, DK-2100 Copenhagen, Denmark.
E-mail: akjaer@sund.ku.dk
Published online Sep. 17, 2015.

^{18}F-FVIIai measured by PET was correlated with TF expression measured ex vivo to confirm specific imaging of tumor TF expression.

MATERIALS AND METHODS

All chemicals were obtained from Sigma Aldrich unless stated otherwise. FVIIai was from Novo Nordisk A/S and was obtained by inactivation of FVIIa with phenylalanine–phenylalanine–arginine–chloromethyl ketone as previously described (*16*). Gly-gly buffer consisted of 10 mM gly-gly, 150 mM NaCl, and 10 mM $CaCl_2$, adjusted to pH 7.5. 4-(ethoxycarbonyl)-*N,N,N*-trimethylbenzenaminium triflate was purchased from ABX. Solid-phase extraction cartridges were obtained from Waters. The PD-10 desalting column was obtained from GE Healthcare. All chemicals were used without further purification.

Cell Culture

BxPC-3 (CRL-1687; American Type Culture Collection [ATCC]) (LGC Standards), HT-29 (HTB-38; ATCC) (LGC Standards), and A2780 cells (catalog no. 93112517; European Collection of Cell Cultures) were cultured in RPMI-1640 (BxPC-3 and A2780) and McCoy's 5a Medium Modified (HT-29) supplemented with 10% fetal bovine serum and 1% penicillin–streptomycin (Invitrogen) at 37°C and 5% CO_2. Cells were tested negative for *Mycoplasma* and a panel of murine pathogens.

Subcutaneous Tumor Xenograft Models

Cells in their exponential growth phase were harvested by trypsinization at 80%–90% confluence and resuspended in 50% Matrigel (BD Biosciences) in complete medium. Tumors were generated in female NMRI nude mice (Taconic) on each flank above the hind limbs by subcutaneous injection of 5×10^6 cells in 100 μL. Tumor growth was monitored twice a week by caliper measurements. Small-animal PET/CT imaging was performed when the tumor volumes were about 150–300 mm^3. All animal experiments were performed under a protocol approved by the National Animal Experiments Inspectorate.

Radiochemistry

Dried ^{18}F-SFB was produced using a 3-step 1-pot procedure as previously described (*17,18*). FVIIai (1.0 mg in 400 μL of *N*-(2-hydroxyethyl)piperazine-*N*-(2-ethanesulfonic acid) buffer, pH 7.5) was added to the dried ^{18}F-SFB and stirred for 1 h at room temperature to yield ^{18}F-FVIIai. The product was purified using a PD-10 desalting column and eluted with gly-gly buffer (pH 7.5).

The product was analyzed by high-performance liquid chromatography using a C4 Grace Vydac column (250 × 4.6 mm). A gradient system with the following parameters was used: 0%–100% B over 25 min, with mobile phase A, 1:9 MeCN/H_2O, 0.1% trifluoroacetic acid, and mobile phase B, 9:1 MeCN/H_2O, 0.1% trifluoroacetic acid, flow rate 1 mL/min.

Protein precipitation was performed as previously described (*18,19*).

Affinity Binding

Surface plasmon resonance (Biacore X100; GE Healthcare) was applied to measure the affinity of ^{18}F-FVIIai binding to TF. TF was coupled to a CM5 chip by amine chemistry as previously reported (*20*). Binding of ^{18}F-FVIIai (12.5–200 nM) to TF was analyzed in 10 mM glycylglysine, 150 mM NaCl, 10 mM $CaCl_2$, and 0.05% surfactant P20 as running buffer. Coupling and dissociation times were set to 180 and 900 s, and the chip was regenerated between samples with 100 mM ethylenediaminetetraacetic acid, pH 7.5, for 240 s. Binding data were analyzed using Biacore X100 Evaluation software (version 2.0.1).

Small-Animal PET/CT

Small-animal PET imaging was performed on a microPET Focus 120 scanner (Siemens). Static images were acquired 1, 2, and 4 h (acquisition time, 480, 600 and 1,200 s, respectively) after intravenous injection of ^{18}F-FVIIai (7.3–9.3 MBq) in 160 μL. Animals received about 37 μg of ^{18}F-FVIIai and were anesthetized by sevoflurane during injections and imaging sessions. Data were acquired in list-mode, and the images were reconstructed using the 3-dimensional maximum a posteriori algorithm with a voxel size of 0.3 × 0.3 × 0.8 mm and a spatial resolution at the center of the field of view of 1.2 mm. No attenuation correction was applied.

CT images were acquired on a microCAT II tomograph (Siemens Medical Systems) after PET imaging. Images were acquired at 360 views with 400-ms exposure at 500 μA and 65 kVp and reconstructed with an isotropic voxel size of 89 μm.

All images were analyzed offline using Inveon software (Siemens Medical Solution). PET and CT images were coregistered and regions of interest (ROIs) drawn over the tumors, liver, kidneys, and muscle to quantify the uptake of ^{18}F-FVIIai expressed as percentage injected dose per gram of tissue (%ID/g).

Biodistribution and Competition with Unlabeled Ligand

Mice were euthanized after the last imaging session and their tumors and organs excised, weighted, and counted in a γ-counter (Wizard2; PerkinElmer) for conventional ex vivo biodistribution. Immediately after γ-counting, tumors were divided and one half was snap-frozen in liquid nitrogen and stored at −80°C. The other half was fixed in 4% neutral buffered formaldehyde for 24 h and transferred to 70% ethanol for molecular analysis.

A competition study with unlabeled FVIIai was performed with a second set of mice. Tumor-bearing mice were divided into 2 groups receiving 500 μg of FVIIai in 150 μL ($n = 3$) or 150 μL of saline alone ($n = 3$) before injection of 5.1–9.6 MBq of ^{18}F-FVIIai by the tail vein 30 min later. Small-animal PET/CT images were acquired 4 h after injection of ^{18}F-FVIIai, and the tumors were subsequently removed for ex vivo γ-counting.

Additional small-animal PET/CT imaging with ^{18}F-FVIIai was performed in a panel of subcutaneous tumor mouse models (A2780, HT-29, and BxPC-3) as a separate experiment. Mice ($n = 4$ per tumor model) were injected with 4.4–10.8 MBq of ^{18}F-FVIIai by the tail vein. Small-animal PET/CT imaging was performed 4 h after injection on an Inveon Multimodality PET/CT scanner (Siemens). Tumors were resected and preserved for molecular analysis after the imaging session as described above.

Tumor Homogenate

Tumor tissues were weighted, and 1 mL of 1x RIPA lysis buffer (Cell Signaling Technology) supplemented with protease inhibitors (Complete Protease Inhibitor Cocktail Tablets; Roche) was added per 100 mg of tumor tissue. Tissue samples were homogenized 2 × 2 min at 30 Hz (Tissue Lyser II; Qiagen), followed by centrifugation at 14,000*g* for 10 min. The supernatant was collected, and the total protein concentration was determined with the BCA assay using the manufacturer's protocol (Micro BCA Protein Assay Kit; Thermo Scientific).

Quantification of TF by Enzyme-Linked Immunosorbent Assay (ELISA)

The TF protein concentration was measured in tumor homogenates by ELISA using the manufacturer's protocol (Tissue Factor DuoSet, catalog no. DY2339; R&D Systems). Standards were applied in duplicate in the range 7.8–500 pg/mL, and a standard curve was fitted to a 3-parameter dose–response curve (Prism 6.0 d; GraphPad Software). Samples were diluted 1:500 and measured in duplicate and the TF concentration interpolated from the standard curve. Finally, the TF concentration was normalized to total protein concentration.

Immunohistochemistry

Formalin-fixed tumors were embedded in paraffin, sectioned into 4-μm slices, and placed on SuperFrost ULTRA PLUS slides (Thermo Scientific) for immunohistochemical staining. Briefly, tissue sections were deparaffinized, rehydrated in a series of alcohols, and submersed

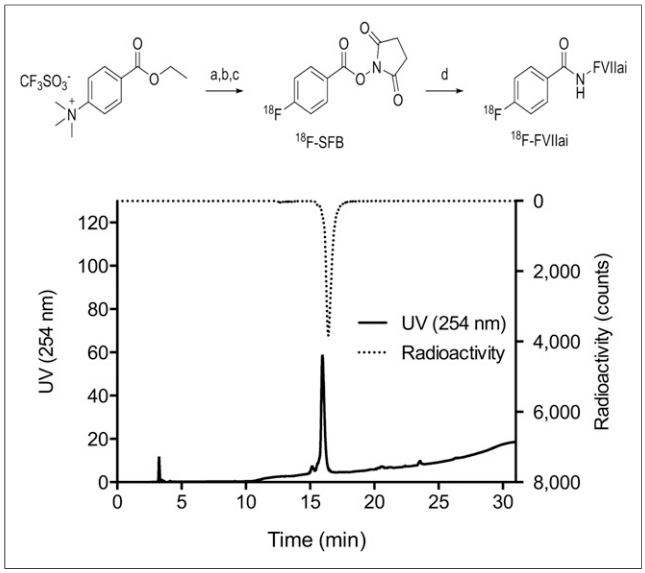

FIGURE 1. (Top) Synthesis of ^{18}F-FVIIai: (a) DMSO, 90°C, 10 min; (b) TPAH, MeCN, 120°C, 6 min; (c) TSTU, MeCN, 90°C, 10 min; and (d) FVIIai (1.29 mg in 500 μL of *N*-(2-hydroxyethyl)piperazine-*N*-(2-ethanesulfonic acid) buffer, pH 7.8). (Bottom) Chromatogram of purified ^{18}F-FVIIai in gly-gly buffer pH 7.5. DMSO = dimethyl sulfoxide; TPAH = tetrapropylammonium hydroxide; TSTU = *O*-(*N*-succinimidyl)-*N,N,N,N*-tetramethyluronium tetrafluoroborate; UV = ultraviolet.

in citrate buffer (pH 6) for heat-induced epitope retrieval by microwave preparation (100°C, 15 min). Sections were washed in phosphate-buffered saline and polysorbate20 and treated with a Peroxidase Blocking Solution (no. S2023; Dako) for 8 min. Subsequently, sections were blocked with 2% bovine serum albumin in phosphate-buffered saline for 10 min. Primary antibody against human tissue factor CD142 (no. 4508; American Diagnostica Inc.) diluted (1:800) in 2% bovine serum albumin was left to incubate for 1 h at room temperature. Primary antibody was detected by the EnVision+ System-HRP Labeled Polymer (no. K4001; Dako) by incubation for 30 min at room temperature. Staining was completed with the Liquid DAB+ Substrate Chromogen System (no. K3468; Dako) and Mayer's Hematoxylin (no. 854183; Region H Apotek) for counterstain.

Statistical Analysis

Unless stated otherwise, data are expressed as mean ± SEM. The Student *t* test or 1-way ANOVA with multiple-comparisons test (Tukey) was applied to compare uptake values, and linear regression analyses were performed to investigate correlations. Data were log-transformed to obtain data with normal distribution and equal variance between groups if necessary. *P* values of 0.05 or less were considered statistically significant. Statistical analyses were performed using GraphPad Prism 6.0 d.

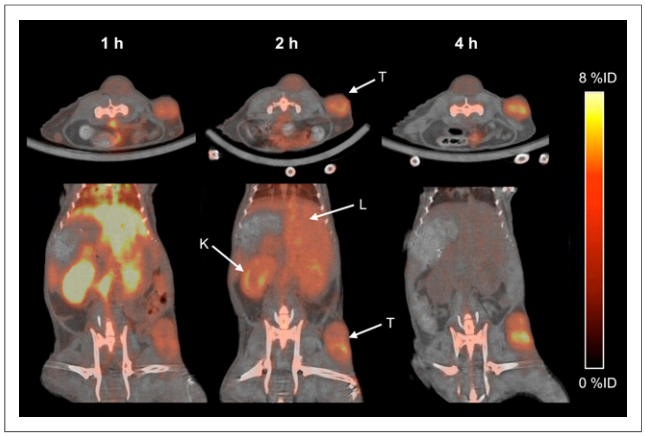

FIGURE 2. Representative transverse and coronal PET/CT images of same mouse imaged at 1, 2, and 4 h after injection of ^{18}F-FVIIai. Arrows point to liver (L), kidney (K), and tumor (T).

RESULTS

Radiochemistry

^{18}F-FVIIai was produced in a 4-step procedure and purified (Fig. 1). The radiochemical yield from ^{18}F was 11.7% ± 0.7%, with a specific radioactivity of 23 ± 6 GBq/μmol. The concentration of FVIIai was 180 ± 50 μg/mL (determined from high-performance liquid chromatography) in 2.75 ± 0.35 mL gly-gly buffer, giving a protein mass of 478 ± 75 μg in the sample. The purity of ^{18}F-FVIIai was 94% ± 5% and 86% ± 8% assessed by high-performance liquid chromatography and protein precipitation, respectively.

Affinity

The affinity of ^{18}F-FVIIai to TF was measured by surface plasmon resonance to ensure that the affinity was not compromised by the procedures applied. Kinetic analysis of the binding data estimated the association and disassociation rates to be 5.0×10^{-5} $M^{-1}s^{-1}$ and $5.6 \times 10^{-4}s^{-1}$, yielding an equilibrium dissociation constant of 1.2 ± 0.3 nM (mean ± SD, $n = 3$).

Small-Animal PET/CT

The in vivo performance of ^{18}F-FVIIai as a PET tracer for imaging was evaluated in mice with subcutaneous BxPC-3 tumors. Small-animal PET/CT images were obtained 1, 2, and 4 h after intravenous injection of ^{18}F-FVIIai. Transverse and coronal sections of the same mouse at 1, 2, and 4 h are shown in Figure 2. At 1 h, the images show high retention of ^{18}F-FVIIai in the vasculature and highly perfused organs such as liver and kidneys, with comparatively low retention in the tumor regions. ^{18}F-FVIIai is cleared predominantly through the kidneys, and an increased tumor-to-tissue contrast was evident at 2 h. At 4 h most of the tracer was cleared whereas the uptake in the tumors remained high, giving rise to a high tumor-to-tissue contrast. In addition, ^{18}F-FVIIai accumulated in joint regions throughout the mice.

Quantitative ROI analysis of liver, kidney, muscle, and tumor uptake was performed to investigate the temporal uptake of ^{18}F-FVIIai. The mean uptake in the tumors remained constant at approximately 2.5 %ID/g over time, whereas the maximum uptake increased from 5.4 ± 0.5 %ID/g at 1 h to 7.1 ± 0.7 %ID/g at 4 h (Fig. 3A). From 1 to 4 h, the uptake in the liver, kidneys, and muscle decreased from 8.7 ± 0.2, 8.9 ± 0.3, and 0.7 ± 0.1 %ID/g to 1.8 ± 0.1, 1.4 ± 0.2, and 0.2 ± 0.01 %ID/g, respectively. At 4 h, the tumors were the tissue with the highest tracer uptake (Fig. 3B).

Biodistribution and Competition with Unlabeled Ligand

Ex vivo biodistribution was performed after the last imaging session to further evaluate the distribution of ^{18}F-FVIIai and validate the imaging results. In concordance with the PET results, tumors had the highest uptake (2.6 ± 0.2 %ID/g) followed by bone (2.0 ± 0.2 %ID/g). Uptake in all other organs was below 2 %ID/g as shown in Figure 4A.

A competition study with preinjection of an excess amount of unlabeled FVIIai was performed in a separate experiment with mice bearing BxPC-3 tumors. The tumor uptake measured ex vivo was significantly reduced in mice preinjected with FVIIai, compared with control mice (1.4 ± 0.1 %ID/g vs. 2.9 ± 0.1 %ID/g, $P \leq 0.001$) as shown in Figure 4B. The reduction in tumor uptake was also clearly

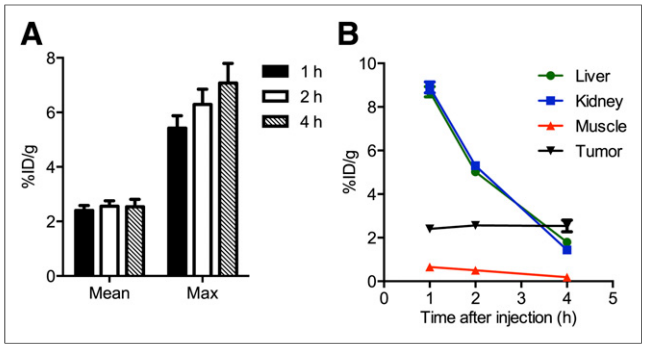

FIGURE 3. Quantitative temporal image analysis of ^{18}F-FVIIai uptake. (A) Mean and maximum (Max) uptake expressed as %ID/g within tumors 1, 2, and 4 h after injection (n = 10). (B) Image-derived biodistribution of ^{18}F-FVIIai in major organs at 1, 2, and 4 h after injection (n = 5).

visible on the in vivo PET images (Fig. 5A). This reduction was confirmed by ROI analysis of the maximum tumor uptake that was significantly reduced in mice preinjected with an excess of FVIIai (2.7 ± 0.1 %ID/g vs. 7.0 ± 0.6 %ID/g, $P \leq 0.001$). In contrast, ROI analysis over the knee joints revealed that preinjection of FVIIai did not affect the maximum ^{18}F-FVIIai uptake in the joints (Fig. 5B).

Correlation of ^{18}F-FVIIai Tumor Uptake and TF Expression

Tumors imaged with ^{18}F-FVIIai were resected to investigate the relationship between uptake of ^{18}F-FVIIai and TF expression in the tumors. The presence of TF and the spatial localization in the tumors were visualized by immunohistochemistry.

A significant positive correlation between TF expression measured ex vivo in tumor homogenates by ELISA and the uptake of ^{18}F-FVIIai quantified by ROI analysis of the PET images was found (Fig. 6). A significant positive correlation was obtained for both the mean (Fig. 6A; $P \leq 0.035$, $r = 0.67$) and the maximum (Fig. 6B; $P \leq 0.019$, $r = 0.72$) ^{18}F-FVIIai uptake at 4 h as a function of the normalized TF protein concentration. Significant positive correlations were also found between TF expression and the quantitative PET measurements at 1 h as well as at 2 h (Supplemental Fig. 1; supplemental materials are available at http://jnm.snmjournals.org).

Immunohistochemistry of paraffin-embedded tumor sections showed strong staining for TF expression in the tumors (Figs. 6C and 6D). The staining was rather heterogeneous, where especially

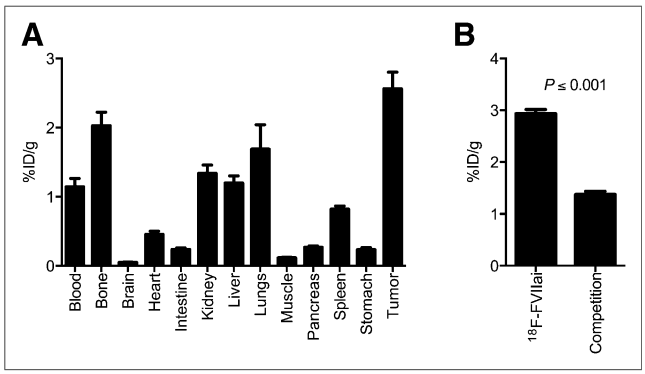

FIGURE 4. (A) Biodistribution of ^{18}F-FVIIai 4 h after injection measured ex vivo (n = 4). (B) Tumor uptake of ^{18}F-FVIIai with and without competition with unlabeled FVIIai measured ex vivo (n = 6).

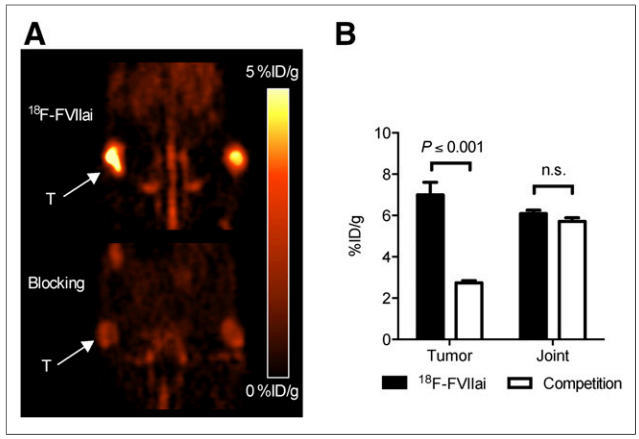

FIGURE 5. (A) Representative coronal PET images of 2 mice imaged 4 h after injection of ^{18}F-FVIIai. Bottom mouse received preinjection of excess unlabeled FVIIai. (B) Quantitative ROI analysis of maximum uptake of ^{18}F-FVIIai in tumors (T) and joints with and without competition. n.s. = not significant.

the cells facing tumor stroma showed strong staining colocalized with the cell membrane.

PET imaging with ^{18}F-FVIIai was repeated in a panel of subcutaneous xenograft mouse models with different expression levels of TF to confirm the ability to image TF expression. Flow cytometry was performed to evaluate the cell surface TF expression before tumor inoculation (Supplemental Materials and Methods and Supplemental Fig. 2). The ovarian carcinoma cell line A2780 was TF-negative, and the colorectal adenocarcinoma cell line was weakly TF-positive. As expected, the BxPC-3 cell line was strongly TF-positive.

Visual inspection of the PET images showed low tumor uptake in the A2780 and HT-29 models, compared with the TF-positive BxPC-3 model (Fig. 7A). The average tumor uptake determined by ROI analysis was significantly different between the 3 models (Fig. 7B; $P \leq 0.01$). The A2780 model had the lowest ^{18}F-FVIIai uptake (0.9 ± 0.1 %ID/g) followed by the HT-29 model (1.6 ± 0.1 %ID/g) and BxPC-3 model (2.2 ± 0.2 %ID/g). TF expression measured ex vivo in tumor homogenates by ELISA was also significantly different among the 3 models (Fig. 7C; $P \leq 0.01$). The A2780 and HT-29 models both had low TF content (0.5 ± 0.01 and 1.8 ± 0.3 pg/μg) whereas the BxPC-3 model had high TF content (47 ± 10 pg/μg). Immunohistochemistry confirmed the expression levels. Both the A2780 and the HT-29 models showed low TF staining (Supplemental Fig. 3) compared with the BxPC-3 model (Figs. 6C and 6D).

DISCUSSION

With the newly developed therapies targeting TF currently moving into clinical trials (ALT-836, NCT01325558; HuMax-TF-ADC, NCT02001623; MORAb-066, NCT01761240) it becomes important to develop diagnostic procedures that aid the oncologists to identify cancer patients eligible for anti-TF therapy. Current methods for assessment of tumor TF status rely on tissue samples and are inherently prone to sampling error, especially in the case of metastatic disease. In contrast, PET allows for imaging of the whole body and enables specific and quantitative measurements of, for example, receptor density. Here we report, to our knowledge, the first use of ^{18}F-labeled FVIIai for noninvasive PET imaging of TF expression.

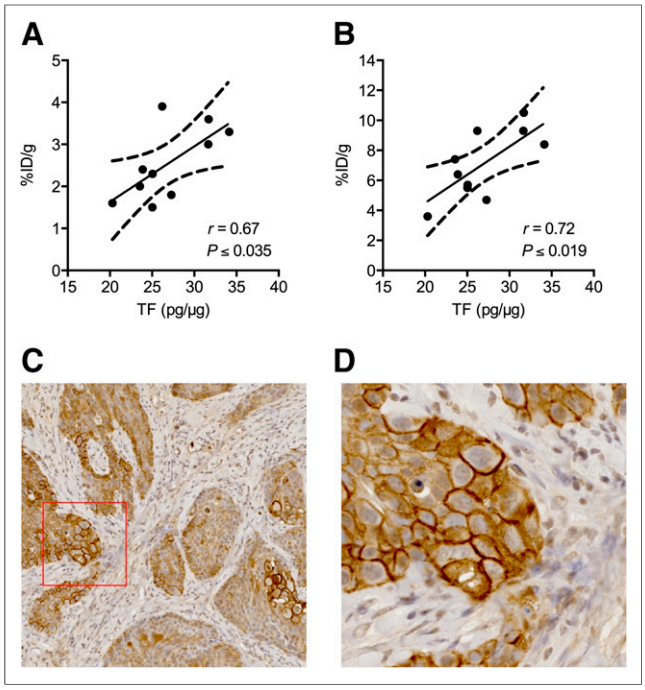

FIGURE 6. Correlation between normalized TF protein concentrations measured in tumor homogenates by ELISA and mean (A) and maximum (B) uptake of ^{18}F-FVIIai within tumors determined by image analysis of PET images acquired 4 h after injection of ^{18}F-FVIIai. Immunohistochemistry shows strong staining for TF in tumor sections (C). (D) High magnification of area marked by red box in C.

Our group has previously described labeling of activated FVII with the SPECT isotopes ^{99m}Tc and ^{111}In for imaging of acute bleeding (*19,21*). Only a few other studies have focused on TF imaging. Temma et al. reported the use of a ^{99m}Tc-labeled anti-TF antibody for ex vivo imaging of macrophage-rich atheromatous lesions in rabbits (*22*). More recently, Hong et al. reported the first use of PET imaging of TF expression in subcutaneous xenograft mouse models using a ^{64}Cu-labeled anti-TF antibody (^{64}Cu-NOTA-ALT-836) (*23*). In the highly TF-expressing BxPC-3 model, imaging with ^{64}Cu-NOTA-ALT-836 led to a high tumor uptake of 5.7 ± 1.8, 10.4 ± 0.8, and 16.5 ± 2.6 %ID/g at 4, 24, and 48 h after injection, respectively. In comparison, we report a mean BxPC-3 tumor uptake of 2.5 ± 0.3 %ID/g 4 h after injection of ^{18}F-FVIIai. The lower tumor uptake can be attributed to the faster pharmacokinetics of ^{18}F-FVIIai than full-length antibodies. The faster pharmacokinetics possibly limit ^{18}F-FVIIai tumor binding because of low availability in the circulating blood. Recently, Shi et al. published the results on the antibody Fab fragment of ALT-836 labeled with ^{64}Cu for PET imaging of TF in a TF-positive triple-negative breast cancer xenograft mouse model (*24*). The reported maximum uptake in TF-positive tumors was 5.1 %ID/g, which was, hence, significantly lower than previously reported with the full-length antibody. This is in line with the results published by Viola-Villegas et al. in which they compared the pharmacokinetics, tumor uptake, and tumor contrast of the ^{89}Zr-labeled anti–prostate-specific member antigen huJ591 antibody and its engineered antibody fragments (*25*). Despite similar K_d values of the ^{89}Zr-huJ591 mAb and its engineered fragments, the tumor uptake of the full-length huJ591 antibody was 3-fold higher relative to its fragments in prostate-specific member antigen–positive tumors. However, the tumor contrast or tumor-to-background ratios were similar between the full-length antibody and the fragments because of faster pharmacokinetics and clearance from nontarget organs and the circulation.

Compared with ^{64}Cu-NOTA-ALT-836, we obtained a superior tumor-to-liver and a tumor-to-muscle ratio of 1.4 ± 0.2 and 13.6 ± 1.6 already 4 h after injection. In the case of ^{18}F-FVIIai, the tumors had the highest uptake compared with any organ 4 h after injection.

The plasma half-life of FVIIai has been reported to be approximately 45 min in rabbits (*26*) and about 4 h in patients (*27*). The shorter distribution time of ^{18}F-FVIIai than antibodies such as ^{64}Cu-NOTA-ALT-836 enables the use of the shorter-lived ^{18}F PET isotope with its superior β^+ branching fraction (^{18}F = 0.97, ^{64}Cu = 0.18) and comparatively better radiodosimetry. As highlighted by others (*25*), the faster pharmacokinetics enable same-day imaging, which will enhance the clinical utility of ^{18}F-FVIIai as a PET tracer.

Surface plasmon resonance analysis of the interaction between ^{18}F-FVIIai and TF was performed to ensure that the radiolabeling did not affect the affinity of FVIIai for TF. The affinity measured after radiolabeling was similar to reported values of unlabeled FVIIai (*28*), indicating no interference with TF binding caused by the radiolabeling.

The uptake of ^{18}F-FVIIai within the tumors was rather heterogeneous as indicated by the large difference between the mean and maximum tumor uptake, 2.5 ± 0.3 and 7.1 ± 0.7 %ID/g at 4 h. We observed a homogeneous TF expression on the cell surface of the BxPC-3 cell in vitro (Supplemental Fig. 2). However, the heterogeneous ^{18}F-FVIIai uptake was in agreement with the highly heterogeneous TF expression pattern observed by us using

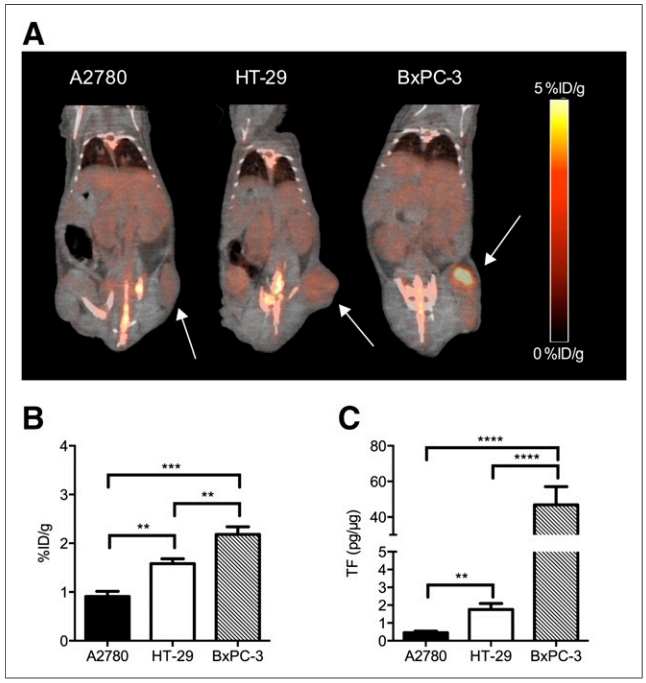

FIGURE 7. (A) Representative coronal PET/CT images of subcutaneous xenograft mouse models with different expression levels of TF imaged 4 h after injection of ^{18}F-FVIIai. Arrows point to tumors. (B) Quantitative ROI analysis of mean uptake of ^{18}F-FVIIai in tumors. (C) TF protein concentrations measured in tumor homogenates by ELISA. $^{**}P \leq 0.01$. $^{***}P \leq 0.001$. $^{****}P \leq 0.0001$.

immunohistochemical staining of tumor sections and is also in agreement with previous findings (*29,30*).

Quantitative analysis of the PET images obtained at 1, 2, and 4 h after injection revealed a constant mean uptake of about 2.5 %ID/g. In contrast, we observed increasing maximum uptake values within the tumors. The physiologic basis for this observation is likely the relationship between tumor perfusion and tumor uptake (*25,31*). At the early time points when the tracer is relatively abundant in the circulation, nonspecific uptake will be observed in areas of the tumor with high perfusion. This will contribute to the measured mean tumor uptake. The nonspecific contribution to the mean tumor uptake will decrease as the tracer is eliminated while increased specific accumulation is observed in areas of high target expression contributing to an increase in maximum uptake within the tumor region.

We report the ability of using ^{18}F-FVIIai for specific in vivo imaging of TF expression. The specific nature of the imaging probe is supported by the competition experiment that shows significant reduction of tumor uptake in mice that received a competition dose of FVIIai before ^{18}F-FVIIai. In addition, ex vivo measurements of total TF content in tumor homogenates correlated with ^{18}F-FVIIai uptake in tumor regions. In vivo ^{18}F-FVIIai PET imaging of TF-negative and weakly TF-positive tumor mouse models further confirmed the specific and TF-mediated uptake of ^{18}F-FVIIai.

The heterogeneous uptake patterns observed on the PET images of BxPC-3 tumors were supported by immunohistochemical staining of tumor sections that showed heterogeneous expression of TF. Strong cell membrane TF staining was seen in focal areas, especially those facing the stromal compartment.

In addition to a high uptake of ^{18}F-FVIIai in the tumors, we noted an accumulation in the joint regions as previously described for ^{125}I-FVIIa in biodistribution studies in a rat model (*32*). Most likely this was due to a nonspecific interaction. This is supported by the image-based analysis of the maximum joint uptake in the competition experiment in which we did not see a reduced joint uptake in the mice receiving unlabeled FVIIai before ^{18}F-FVIIai.

A limitation of the study is the absence of human TF outside the tumor regions in the xenograft mouse model applied. It has previously been shown that the cross-species compatibility for TF/FVII is rather low such that human FVIIai binds with much lower affinity to murine than to human TF (*28,33*). Hence, the current mouse model is possibly underestimating the background uptake of FVIIai to be seen in human tissues. Still immunohistochemical studies showing high expression of TF in human tumors relative to the background expression (*5–8*) hold promise for a future application in cancer patients. A test in another animal model with a better cross-species compatibility between TF and human FVIIai allows for a more optimal evaluation of ^{18}F-FVIIai tumor uptake in the presence of background target expression and could be a logical next step before clinical translation.

In our work we report a specific activity for ^{18}F-FVIIai of 23 GBq/μmol. With a radioactive dose comparable to that of an ^{18}F-FDG PET scan, a 75-kg patient would receive a dose of 375 MBq, which corresponds to a mass dose of less than 0.01 mg of ^{18}F-FVIIai per kilogram or less than 0.75 mg of ^{18}F-FVIIai for a 75-kg patient. FVIIai has previously been evaluated in clinical trials as an anticoagulant, and administration of FVIIai in a single dose of up to 0.40 mg/kg of body weight was found to be safe and without increased risk of bleeding events (*27,34,35*). Hence we do not expect toxicity issues related to the mass amount of FVIIai when administering ^{18}F-FVIIai in the clinical setting. Also, ^{18}F-SFB has been successfully tested clinically for antibody-based PET imaging (*36*). This safety profile together with its highly specific uptake in TF-positive tumors argues for translation into clinical testing in patients of TF PET imaging using ^{18}F-FVIIai.

CONCLUSION

^{18}F-FVIIai was found to be a valuable tool for specific and noninvasive PET imaging of tumor TF expression. High uptake of ^{18}F-FVIIai was seen in TF-positive tumors 4 h after injection, and the uptake of ^{18}F-FVIIai correlated with TF expression measured ex vivo in tumor homogenates. These characteristics of ^{18}F-FVIIai merit its further development and clinical translation as a TF-specific PET imaging agent with potential as a companion diagnostic for emerging TF-targeted therapies.

DISCLOSURE

The costs of publication of this article were defrayed in part by the payment of page charges. Therefore, and solely to indicate this fact, this article is hereby marked "advertisement" in accordance with 18 USC section 1734. The current work was supported by a grant from Innovation Fund Denmark, the John and Birthe Meyer Foundation, Novo Nordisk Foundation, Lundbeck Foundation, AP Møller Foundation, Svend Andersen Foundation, the Arvid Nilsson Foundation, Research Council for Independent Research, Research Council of Rigshospitalet, and Research Foundation of the Capital Region of Denmark. Lars C. Petersen is an employee of Novo Nordisk A/S. No other potential conflict of interest relevant to this article was reported.

ACKNOWLEDGMENTS

We thank Michelle Kaijer for excellent technical assistance and the Cyclotron team at Rigshospitalet for flexible production of ^{18}F.

REFERENCES

1. van den Berg YW, Osanto S, Reitsma PH, Versteeg HH. The relationship between tissue factor and cancer progression: insights from bench and bedside. *Blood.* 2012;119:924–932.
2. Ruf W, Yokota N, Schaffner F. Tissue factor in cancer progression and angiogenesis. *Thromb Res.* 2010;125(suppl 2):S36–S38.
3. Kasthuri RS, Taubman MB, Mackman N. Role of tissue factor in cancer. *J Clin Oncol.* 2009;27:4834–4838.
4. Ruf W, Mueller BM. Thrombin generation and the pathogenesis of cancer. *Semin Thromb Hemost.* 2006;32(suppl 1):61–68.
5. Ueno T, Toi M, Koike M, Nakamura S, Tominaga T. Tissue factor expression in breast cancer tissues: its correlation with prognosis and plasma concentration. *Br J Cancer.* 2000;83:164–170.
6. Seto S, Onodera H, Kaido T, et al. Tissue factor expression in human colorectal carcinoma: correlation with hepatic metastasis and impact on prognosis. *Cancer.* 2000;88:295–301.
7. Khorana AA, Ahrendt SA, Ryan CK, et al. Tissue factor expression, angiogenesis, and thrombosis in pancreatic cancer. *Clin Cancer Res.* 2007;13:2870–2875.
8. Förster Y, Meye A, Albrecht S, Schwenzer B. Tissue factor and tumor: clinical and laboratory aspects. *Clin Chim Acta.* 2006;364:12–21.
9. Nitori N, Ino Y, Nakanishi Y, et al. Prognostic significance of tissue factor in pancreatic ductal adenocarcinoma. *Clin Cancer Res.* 2005;11:2531–2539.
10. Kakkar AK, Lemoine NR, Scully MF, Tebbutt S, Williamson RC. Tissue factor expression correlates with histological grade in human pancreatic cancer. *Br J Surg.* 1995;82:1101–1104.
11. Yu JL, May L, Lhotak V, et al. Oncogenic events regulate tissue factor expression in colorectal cancer cells: implications for tumor progression and angiogenesis. *Blood.* 2005;105:1734–1741.
12. Hu Z, Sun Y, Garen A. Targeting tumor vasculature endothelial cells and tumor cells for immunotherapy of human melanoma in a mouse xenograft model. *Proc Natl Acad Sci USA.* 1999;96:8161–8166.
13. Ngo CV, Picha K, McCabe F, et al. CNTO 859, a humanized anti-tissue factor monoclonal antibody, is a potent inhibitor of breast cancer metastasis and tumor growth in xenograft models. *Int J Cancer.* 2007;120:1261–1267.

14. Versteeg HH, Schaffner F, Kerver M, et al. Inhibition of tissue factor signaling suppresses tumor growth. *Blood.* 2008;111:190–199.
15. Breij ECW, de Goeij BECG, Verploegen S, et al. An antibody-drug conjugate that targets tissue factor exhibits potent therapeutic activity against a broad range of solid tumors. *Cancer Res.* 2014;74:1214–1226.
16. Sorensen BB, Persson E, Freskgård PO, et al. Incorporation of an active site inhibitor in factor VIIa alters the affinity for tissue factor. *J Biol Chem.* 1997;272: 11863–11868.
17. Tang G, Tang X, Wang X. A facile automated synthesis of N-succinimidyl 4-[^{18}F]fluorobenzoate ([^{18}F]SFB) for ^{18}F-labeled cell-penetrating peptide as PET tracer. *J Labelled Comp Radiopharm.* 2010;53:543–547.
18. Erlandsson M, Nielsen CH, Jeppesen TE, et al. Synthesis and characterization of ^{18}F-labeled active site inhibited factor VII (ASIS). *J Labelled Comp Radiopharm.* 2015;58:196–201.
19. Madsen J, Kristensen JB, Olsen OH, et al. Recombinant coagulation factor VIIa labelled with the fac-99 mTc(CO)3-core: synthesis and in vitro evaluation of a putative new radiopharmaceutical for imaging in acute bleeding lesion. *J Labelled Comp Radiopharm.* 2011;54:214–219.
20. Persson E. Influence of the gamma-carboxyglutamic acid-rich domain and hydrophobic stack of factor VIIa on tissue factor binding. *Haemostasis.* 1996;26 (suppl 1):31–34.
21. Nalla A, Buch I, Sigvardt M, Bodholdt RP, Kjaer A, Hesse B. (^{11}Indium labelling of recombinant activated coagulation factor VII: in vitro and preliminary in vivo studies in healthy rats. *Int J Mol Imaging.* 2012;2012:464810.
22. Temma T, Ogawa Y, Kuge Y, et al. Tissue factor detection for selectively discriminating unstable plaques in an atherosclerotic rabbit model. *J Nucl Med.* 2010;51:1979–1986.
23. Hong H, Zhang Y, Nayak TR, et al. Immuno-PET of tissue factor in pancreatic cancer. *J Nucl Med.* 2012;53:1748–1754.
24. Shi S, Hong H, Orbay H, et al. ImmunoPET of tissue factor expression in triple-negative breast cancer with a radiolabeled antibody Fab fragment. *Eur J Nucl Med Mol Imaging.* 2015;42:1295–1303.
25. Viola-Villegas NT, Sevak KK, Carlin SD, et al. Noninvasive imaging of PSMA in prostate tumors with ^{89}Zr-labeled huJ591 engineered antibody fragments: the faster alternatives. *Mol Pharm.* 2014;11:3965–3973.
26. Cirillo P, Golino P, Ragni M, et al. Long-lasting antithrombotic effects of a single dose of human recombinant, active site-blocked factor VII: insights into possible mechanism(s) of action. *J Thromb Haemost.* 2003;1:992–998.
27. Erhardtsen E, Nilsson P, Johannessen M, Thomsen MS. Pharmacokinetics and safety of FFR-rFVIIa after single doses in healthy subjects. *J Clin Pharmacol.* 2001;41:880–885.
28. Petersen LC, Nørby PL, Branner S, et al. Characterization of recombinant murine factor VIIa and recombinant murine tissue factor: a human-murine species compatibility study. *Thromb Res.* 2005;116:75–85.
29. Müller M, Flössel C, Haase M, et al. Cellular localization of tissue factor in human breast cancer cell lines. *Virchows Arch, B. Cell Pathol.* 1993;64: 265–269.
30. Saito Y, Hashimoto Y, Kuroda J-I, et al. The inhibition of pancreatic cancer invasion-metastasis cascade in both cellular signal and blood coagulation cascade of tissue factor by its neutralisation antibody. *Eur J Cancer.* 2011;47:2230–2239.
31. Niu G, Li Z, Xie J, Le Q-T, Chen X. PET of EGFR antibody distribution in head and neck squamous cell carcinoma models. *J Nucl Med.* 2009;50: 1116–1123.
32. Beeby TL, Chasseaud LF, Taylor T, Thomsen MK. Distribution of the recombinant coagulation factor ^{125}I-rFVIIa in rats. *Thromb Haemost.* 1993;70: 465–468.
33. Knudsen T, Olsen OH, Petersen LC. Tissue factor and factor VIIa cross-species compatibility. *Front Biosci (Landmark Ed).* 2011;16:3196–3215.
34. Jilma B, Marsik C, Mayr F, et al. Pharmacodynamics of active site-inhibited factor VIIa in endotoxin-induced coagulation in humans. *Clin Pharmacol Ther.* 2002;72:403–410.
35. Vincent J-L, Artigas A, Petersen LC, Meyer C. A multicenter, randomized, double-blind, placebo-controlled, dose-escalation trial assessing safety and efficacy of active site inactivated recombinant factor VIIa in subjects with acute lung injury or acute respiratory distress syndrome. *Crit Care Med.* 2009;37:1874–1880.
36. Neumaier B, Mottaghy FM, Buck AK, et al. Short communication: ^{18}F-immuno-PET: determination of anti-CD66 biodistribution in a patient with high-risk leukemia. *Cancer Biother Radiopharm.* 2008;23:819–824.